Cellular/Molecular

Cooperative Interactions between 480 kDa Ankyrin-G and EB Proteins Assemble the Axon Initial Segment

Amélie Fréal,[1,2,3,4] Coralie Fassier,[1,2,3] Barbara Le Bras,[1,2,3] Erika Bullier,[1,2,3] Stéphanie De Gois,[1,2,3] Jamilé Hazan,[1,2,3]* Casper C. Hoogenraad,[4]* and François Couraud[1,2,3]*

[1]Sorbonne Universités, UPMC Université Paris 06, [2]INSERM UMR-S 1130, and [3]CNRS UMR 8246, Neuroscience Paris Seine, F-75005, Paris, France, and [4] Cell Biology, Faculty of Science, Utrecht University, Padualaan 8, CH Utrecht 3584, The Netherlands

The axon initial segment (AIS) is required for generating action potentials and maintaining neuronal polarity. Significant progress has been made in deciphering the basic building blocks composing the AIS, but the underlying mechanisms required for AIS formation remains unclear. The scaffolding protein ankyrin-G is the master-organizer of the AIS. Microtubules and their interactors, particularly end-binding proteins (EBs), have emerged as potential key players in AIS formation. Here, we show that the longest isoform of ankyrin-G (480AnkG) selectively associates with EBs via its specific tail domain and that this interaction is crucial for AIS formation and neuronal polarity in cultured rodent hippocampal neurons. EBs are essential for 480AnkG localization and stabilization at the AIS, whereas 480AnkG is required for the specific accumulation of EBs in the proximal axon. Our findings thus provide a conceptual framework for understanding how the cooperative relationship between 480AnkG and EBs induces the assembly of microtubule-AIS structures in the proximal axon.

Key words: **ankyrin-G; axon initial segment; end-binding protein; microtubule; neuronal polarity**

Significance Statement

Neuronal polarity is crucial for the proper function of neurons. The assembly of the axon initial segment (AIS), which is the hallmark of early neuronal polarization, relies on the longest 480 kDa ankyrin-G isoform. The microtubule cytoskeleton and its interacting proteins were suggested to be early key players in the process of AIS formation. In this study, we show that the crosstalk between 480 kDa ankyrin-G and the microtubule plus-end tracking proteins, EBs, at the proximal axon is decisive for AIS assembly and neuronal polarity. Our work thus provides insight into the functional mechanisms used by 480 kDa ankyrin-G to drive the AIS formation and thereby to establish neuronal polarity.

Introduction

Neurons are highly polarized cells and their activity is built upon their morphological polarity. The directional propagation of signals from the dendrites to the axon relies on the segregation of the somatodendritic and axonal compartments. The axon initial segment (AIS) is the hinge point between these two regions. At this transition point, action potentials are generated to travel along the axon and the integrity of the AIS ensures the establishment and long-term maintenance of neuronal polarity (Kole and Stuart, 2012; Yoshimura and Rasband, 2014). The AIS scaffolding protein ankyrin-G (AnkG) is the master-organizer of the initial axon (Zhou et al., 1998; Hedstrom et al., 2008; Sobotzik et al., 2009). Three neuronal AnkG isoforms have been reported (Kordeli et al., 1995), including the 480 kDa AnkG (480AnkG), which was recently shown to be necessary for AIS formation (Jenkins et al., 2015). However, the cellular and molecular mechanisms underlying 480AnkG-mediated AIS formation remain elusive.

The microtubule (MT) cytoskeleton and its associated proteins play a pivotal role during the different phases of neuronal polarization, regulating several aspects of the establishment and maintenance of neuronal polarity (Kapitein and Hoogenraad,

Received Aug. 24, 2015; revised Feb. 1, 2016; accepted Feb. 4, 2016.

Author contributions: A.F., J.H., C.C.H., and F.C. designed research; A.F., C.F., and B.L.B. performed research; E.B. and S.D.G. contributed unpublished reagents/analytic tools; A.F., C.F., and B.L.B. analyzed data; A.F., C.F., J.H., and C.C.H. wrote the paper.

This work was supported by the Fondation pour la Recherche Médicale and by the Agence Nationale pour la Recherche (HYPER-MND, ANR-2010-BLAN-1429-01) and the Netherlands Organization for Scientific Research (NWO-ALW-VICI to C.C.H.). We thank Jean-François Gilles and Susanne Bolte from the Cell Imaging and Flow Cytometry facility of the IFR83/UPMC (Paris, France) for their assistance in microscopy and image analysis, Sam van Beuningen for his help with the FRAP experiments, Vann Bennett for providing us with rat 190AnkG-GFP and 270AnkG-GFP constructs, and Eric Denarier for the *in silico* analysis of the 480AnkG coding sequence.

The authors declare no competing financial interests.

*J.H., C.C.H., and F.C. contributed equally to this work.

Correspondence should be addressed to either Dr. Amélie Fréal or Casper C. Hoogenraad (for reagents), Cell Biology, Faculty of Science, Utrecht University, Padualaan 8, CH Utrecht 3584, The Netherlands, E-mail: a.freal@uu.nl or c.hoogenraad@uu.nl.

DOI:10.1523/JNEUROSCI.3219-15.2016

 0270-6474/16/364421-13$15.00/0

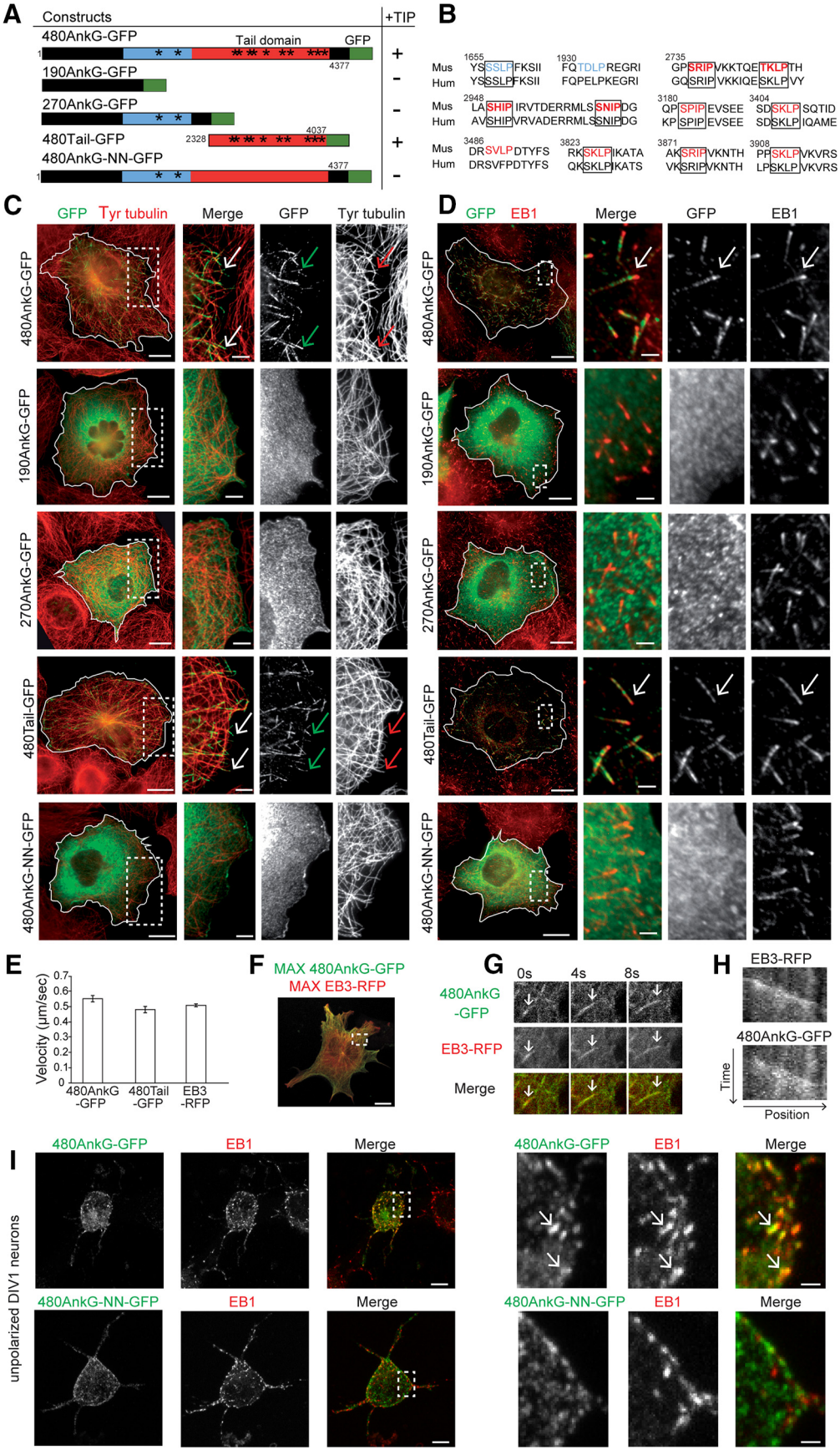

Figure 1. 480AnkG associates with MT plus ends in an EB-dependent manner via its specific tail domain. ***A***, Table illustrating the different AnkG constructs used in this study and their ability to track MT plus ends. Regions specific to 480AnkG, shared by 480 and 270Ank or by all AnkG isoforms are indicated in red, blue, and black respectively. Asterisks pinpoint the position of the SxIP motifs and amino acids at the beginning and the end of each construct are numbered. ***B***, Identification of 10 conserved SxIP motifs (boxed) between the mouse (Mus) (*Figure legend continues.*)

2015). Interestingly, the MT network shows specific properties within the initial axon because MTs appear tightly fasciculated (Palay et al., 1968) and more stable (Gomis-Rüth et al., 2008; Sanchez-Ponce et al., 2011), whereas end-binding proteins (EBs) are unusually accumulated along the MT lattice at the proximal axon (Nakata and Hirokawa, 2003; Leterrier et al., 2011). This particular MT architecture develops very early during the process of AIS formation (Jones et al., 2014). Although a link between AnkG and MTs through EBs has been reported in mature neurons (Leterrier et al., 2011), the physiological significance of this interaction in the context of AIS formation and in the establishment of neuronal polarity has not been investigated.

We here show that the longest isoform of AnkG, 480AnkG, selectively associates with EBs via its specific tail domain, and that this interaction is necessary for the building of the AIS and the establishment of neuronal polarity. Moreover, EBs are required for 480AnkG correct location, and reciprocally 480AnkG is responsible for EB accumulation and MT organization at the nascent AIS. Our analysis thus reveals that the crosstalk between 480AnkG and EBs provides the keystone of AIS-MT assembly in the proximal axon, and unveils the functional mechanism that 480AnkG uses to control AIS formation and thereby to establish neuronal polarity.

Materials and Methods

Animals. The use of female OF1 mice (Charles River Laboratories) and Sprague-Dawley rats (Janvier) followed the guidelines established by the European Animal Care and Use Community (86/609/CEE), the French decree no. 97/748 (J Off République Française, October 20, 1987, pp 12245–12248) as well as the recommendations from the CNRS and Université Pierre and Marie Curie.

Antibodies. A rabbit anti-480AnkG antibody (Eurogentec) was developed against amino acid residues 3516–3530 of the human sequence (NM 020987.3) and diluted at 1:500 for both Western blot and immunocytochemical analyses. The following primary antibodies were used at the respective dilutions: rabbit anti-Pan(SR)AnkG [Ser/Thr-rich (SR); Le Bras et al., 2014; recognizes 270- and 480AnkG] at 1:500, mouse anti-Pan(SBD)AnkG [spectrin-binding domain (SBD); clone N106/65, NeuroMab, recognizes 190-, 270-, and 480AnkG] at 1:500, mouse anti-PanNav (K58/35, Sigma-Aldrich) at 1:200, mouse and chicken anti-MAP2 (HM-2, Sigma-Aldrich and ab5392, Abcam) at 1:500 and 1:5000, mouse anti-Neurofascin (A12/18, NeuroMab) at 1:500, chicken and mouse anti-GFP (Invitrogen) at 1:800 and 1:500, respectively, chicken and rabbit anti-βIV-spectrin (gifts from Masayuki Komada (Tokyo Institute of Technology, Tokyo, Japan) and Maren Engelhardt (Institute of Neuroanatomy, Heidelberg University, Mannheim, Germany); (Komada and Soriano, 2002; Gutzmann et al., 2014) at 1:500, mouse anti-β2-karyopherin (D45, Santa Cruz Biotechnology) at 1:500, mouse anti-EB1 (5/EB1, BD Biosciences) at 1:300, anti-tyrosinated tubulin (TUB-1A2, Sigma-Aldrich) at 1:1000 and mouse anti-Tau-1 (MAB3420, Millipore) at 1:700. The corresponding 350-, 488-, 594-, 568-, or 647-Alexa-conjugated secondary antibodies were from Invitrogen and Cy3.5 anti-chicken was from Jackson ImmunoResearch.

Immunochemistry. Mouse embryos and adult brains were dissected out and fixed by immersion in 2% paraformaldehyde (PFA) for 1 h at 4°C. Adult mice were fixed by intracardiac perfusion with 1% PFA. Spinal cords were dissected and postfixed by immersion in 1% PFA for 1 h at 4°C. Immunostaining was processed on transverse sections of mouse embryos, adult spinal cords, or sagittal sections of adult brains as previously described (Le Bras et al., 2014).

Neurons were fixed at 1 d *in vitro* (DIV1), DIV2, DIV5, or DIV8 for 10 min at room temperature in 2% PFA-4% sucrose, preheated at 37°C. After three washes in PBS, they were permeabilized in 0.1% Triton X-100 in PBS for 10 min, and blocked for 2 h in blocking solution (5% NGS in PBS). Primary antibodies were diluted in the blocking solution and incubated overnight at 4°C. Neurons were then washed three times in PBS and incubated with the appropriate secondary antibodies for 2 h at room temperature. For EB1 and EB3 staining, neurons were fixed for 5 min in methanol at −20°C and postfixed 5 min in 2% PFA-4% sucrose at room temperature. COS-7 cells were fixed in cold methanol for 10 min at −20°C and in 4% PFA-4% sucrose for 10 min at room temperature.

cDNA constructs. The cDNA sequences of the mouse 480AnkG and 270AnkG were determined by aligning the published human 480AnkG (NM 020987.3) and rat 270AnkG (NM 001033984) sequences in the mouse genome database (UCSC genome browser, Genome Assembly: http://genome.ucsc.edu/) and were synthesized by GeneCust. The cDNAs were subcloned into pEGFP-N1 (Clontech) in the KpnI and AgeI restriction cloning sites. These two restriction sites were deleted from the synthesized cDNA without altering the protein sequences. cDNA encoding mutated 480AnkG-GFP was synthetized by replacing the putative EB-binding motifs SxIP of the 480 Tail domain by SxNN (Fig. 1*B*) and cloned into pEGFP-N1 using the same restriction site as for the WT cDNA. EB3-RFP and EB3-GFP were a gift from Annie Andrieux (INSERM U1216, CEA-BIG, Univ. Grenoble Alpes, Grenoble Institut Neurosciences, Grenoble, France; Peris et al., 2006). Rat 190AnkG-GFP and 270AnkG-GFP were kindly provided by Vann Bennett (Duke University Medical Center, Durham, NC; Zhang and Bennett, 1998). Myc-K_v2.1-Na_v1.2 (Kv-Nav) construct was kindly provided by Bénédicte Dargent (Aix Marseille Université, CNRS, CRN2M UMR7286, Marseille, France; Bréchet et al., 2008). ShRNAs were cloned into pSUPER (Oligoengine). The 480AnkG-shRNA sequence was as follows: GTTCAGAGGAAGTGAGTTA. PanAnkG-shRNA was used by Hedstrom et al. (2007) and Leterrier et al. (2011), and EB1/3-shRNA was previously described by Komarova et al. (2005) and Jaworski et al. (2009). Empty pSUPER was used as a control.

Cell culture and transfection. Hippocampal and cortical neurons were prepared from embryonic day 18.5 (E18.5) rat or E17.5 mouse embryos. Neurons were plated on poly-D-ornithine (5 μg/ml) and laminin (2 μg/ml) coverslips. Cultures were grown in neurobasal supplemented with 2%B27 and 1%GlutaMAX, transfected at DIV0–DIV1 using Lipofectamine 2000 (Invitrogen) with a DNA–Lipofectamine ratio of 1:1.15 and fixed at indicated time points. Transfection of the 480Tail-GFP construct systematically led to neuronal death. COS-7 cells were cultured in DMEM with 10% fetal calf serum. Cells were transfected using Lipofectamine 2000 (Invitrogen).

Image acquisition, time-lapse videomicroscopy, and data analysis. Images were acquired using a fluorescence microscope equipped with an Apotome module (Zeiss, Axiovert 200M). Confocal images were acquired using a Confocal Laser Scanning Microscope (Leica TCS SP5 AOBS, Leica Microsystems) equipped with a 63×/1.4 NA oil-immersion objective and a low-noise hybrid detector (HyD, Leica Microsystems). Time-lapse recordings of 480AnkG-GFP, 480Tail-GFP, 270AnkG-GFP, 190AnkG-GFP, and EB3-RFP in COS-7 cells and EB3-GFP in cultured neurons were performed at 37°C, 5% of CO_2 using a Leica DMI 6000B inverted spinning-disk microscope with a 63× immersion objective. Images were acquired every 2 s during 4–5 min. Comet analyses were performed in COS-7 cells using MTrackJ plugin (Fiji) or in neurons using the multiple kymograph plugin (Fiji) and the "read velocities from tsp" (Fiji, J. Rietdorf and A. Seitz) macros for kymograph production and analyses respectively. GFP polarity index was calculated by dividing the

←

(*Figure legend continued.*) and human (Hum) sequences of 480AnkG. Motifs in red are specific to 480AnkG, motifs in blue are shared by 480AnkG and 270AnkG. Bold motifs are repeated in tandem. ***C***, ***D***, COS-7 cells overexpressing the indicated constructs and stained for GFP (green) and tyrosinated tubulin (***C***, red) or EB1 (***D***, red). ***E***, Mean velocity of 480AnkG-GFP ($n = 30$), 480Tail-GFP ($n = 37$), and EB3-RFP ($n = 46$) comets in COS-7 cells. $p > 0.05$, two-tailed unpaired *t* test. Error bars are SEM. ***F***, Maximum *t* projection from a time-lapse recording of COS-7 cells expressing EB3-RFP (red) and 480AnkG-GFP (green). ***G***, ***H***, Representative stills (***G***) and kymograph (***H***) from a time-lapse recording of a single MT plus end colabeled by EB3-RFP (red) and 480AnkG-GFP (green) in COS-7 cells. Vertical and horizontal scale bars represent 60 s and 12 μm, respectively. ***I***, DIV1 rat hippocampal neurons transfected at DIV0 with 480AnkG-GFP or 480AnkG-NN-GFP and stained for GFP (green) and EB1 (red). Right, Enlargements of the boxed areas in the left panel. ***C–I***, Arrows point to MT plus ends. Scale bars: ***C***, ***D***, ***F***, 15 μm; ***I***, 10 μm; magnifications: ***C***, ***D***, 5 μm; ***I***, 1 μm.

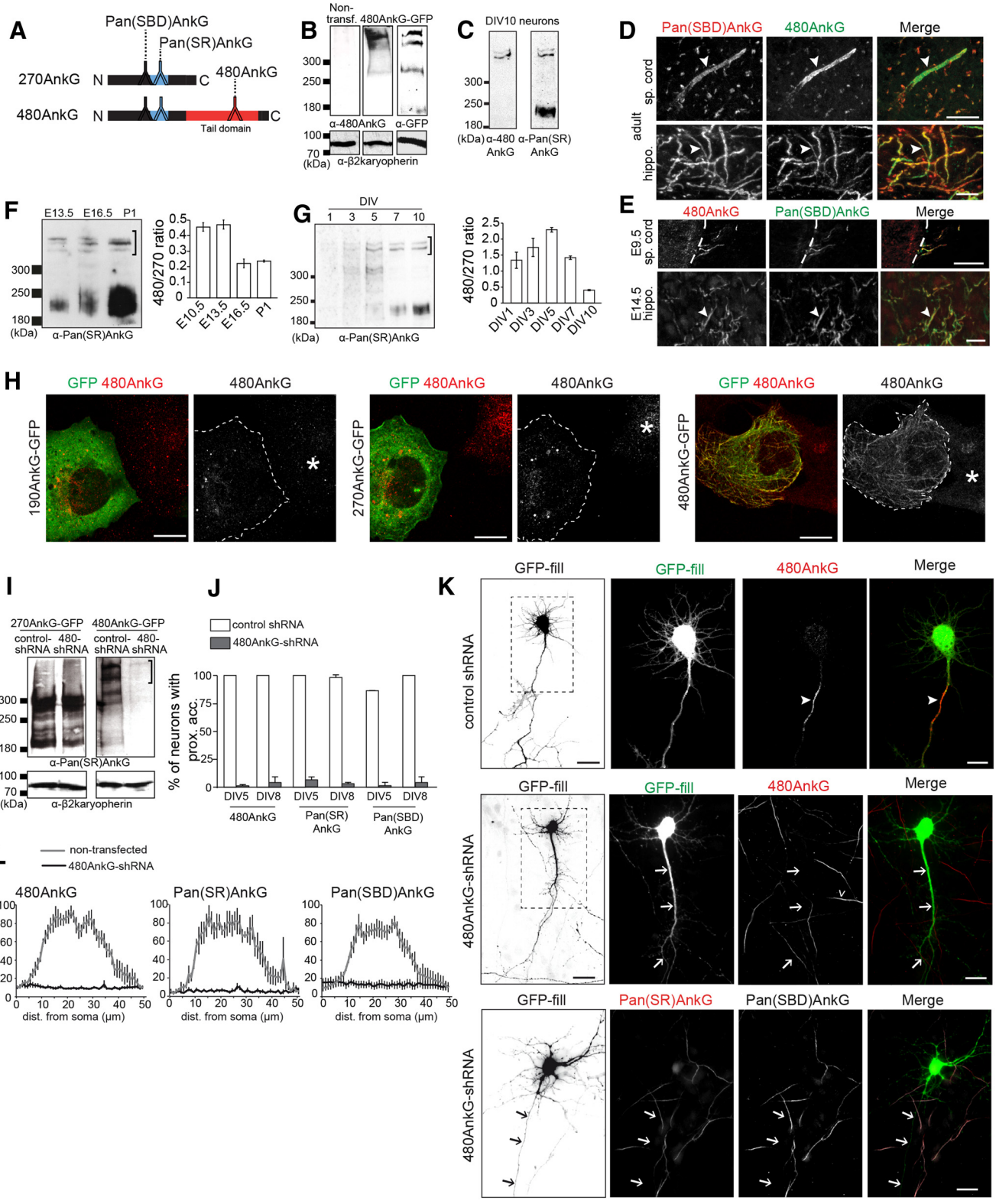

Figure 2. 480AnkG is required for 270- and 190AnkG clustering at the AIS during neuronal development. ***A***, Representative scheme of 270- and 480AnkG, with the epitope positions of the three antibodies used in this study. ***B***, Western-blot analysis of protein extracts from COS-7 cells expressing or not 480AnkG-GFP using 480AnkG or GFP antibodies. β2-karyopherin was used as a loading control. ***C***, Western blot of DIV10 cortical neurons extracts using 480AnkG or Pan(SR)AnkG antibodies. ***D***, Immunolabeling of adult mouse spinal cord (sp. cord) and hippocampus (hippo., CA3 region) sections with Pan(SBD)AnkG (red) and 480AnkG (green) antibodies. ***E***, Immunolabeling of embryonic mouse spinal cord (at E9.5) and hippocampus (E14.5) sections with 480AnkG (in red) and Pan(SBD)AnkG (in green) antibodies. The spinal cord is delimited by a dashed line. ***F***, ***G***, Western blot of E13.5, E16.5, and P1 mouse spinal cords (***F***) and extracts from rat cortical neurons at DIV1, DIV3, DIV5, DIV7, and DIV10 (***G***) stained with Pan(SR)AnkG. Ratios of 480/270AnkG are quantified at indicated stages. The 480AnkG bands used for the quantifications are indicated by brackets. ***H***, Immunolabeling of COS-7 cells transfected with 190-, 270-, or 480AnkG-GFP constructs using GFP (green) and 480AnkG (red) antibodies. Right, The border of transfected cells is framed by a dashed line and the asterisks pinpoint nontransfected cells. ***I***, Western blot on protein extracts from COS-7 cells cotransfected with 270AnkG-GFP or 480AnkG-GFP and control- or 480AnkG-shRNA using Pan(SR)AnkG antibody. β2-Karyopherin was used as a loading control. The specific bands for 480AnkG are shown by a bracket. ***J***, Average percentage of DIV5 and (*Figure legend continues.*)

mean intensity of fluorescence in the first 20 μm of the axon by the mean intensity of fluorescence in the first 20 μm of the dendrites. All data resulted from three independent experiments and are presented as mean ± SEM. Statistical significance of the data were determined using the parametric unpaired two-tailed *t* test or nonparametric Mann–Whitney test. When more than two groups were analyzed, one-way ANOVA or Kruskal–Wallis tests were used followed by Tukey's and Dunn's multiple-comparison tests, respectively (GraphPad).

Fluorescence recovery after photobleaching experiments. For quantitative fluorescence recovery after photobleaching (FRAP) experiments, neurons were transfected as described before, and imaged on an inverted research microscope Nikon Eclipse Ti-E with perfect focus system (PFS, Nikon), equipped with Nikon CFI Apo TIRF 100× 1.49 N.A. oil objective, CoolSNAP HQ2 CCD camera (Roper Scientific), and controlled by MetaMorph 7.7 software (Molecular Devices). The FRAP experiments were performed using the ILas2 system (Roper Scientific). Coverslips (24 mm) were mounted in metal rings and maintained at 37°C and 5% CO_2 in a stage top incubator (INUBG2E-ZILCS; Tokai Hit). For FRAP experiments, a ROI on the proximal axon was photobleached with high laser power. The mean intensity of this region was corrected by subtracting at each frame the mean intensity of a background region next to it.

$$I(t) = I_{\text{bleached region}}(t) - I_{\text{background}}(t)$$

The normalization of recovery $R_{\text{norm}}(t)$ was calculated according to the following formula:

$$R_{\text{norm}}(t) = \frac{I(t) - I(0)}{< I(\Delta t) > - I(0)}$$

where $I(0)$ corresponds to the region's mean intensity directly after bleaching, and $< I(\Delta t) >$ corresponds to the intensity averaged over five initial frames before bleaching. To account for the bleaching due to imaging itself, additional correction was performed using intensity of the nonbleached region along the axon:

$$R(t) = R_{\text{norm}}(t) \frac{< I_{\text{control}}(\Delta t) - I_{\text{background}}(\Delta t) >}{I_{\text{control}}(t) - I_{\text{background}}(t)}$$

where I_{control} corresponds to the mean intensity of the nonbleached region, and time interval Δt denotes five initial frames before bleaching. The recovery curves of at least 10 neurons were pooled together and averaged. The maximum recovery fraction R_{max} was obtained by fitting two-association phase curves in GraphPad Prism.

Western blot analysis. Cultured neurons or dissected spinal cords were homogenized in ice-cold homogenization buffer (5 mM TrisHCl, pH 7.4, 2 mM EDTA and protease inhibitor mixture consisting of 0.5 mM APMSF with leupeptin, aprotinin, and pepstatin A at 1 μg/ml each). These protein extracts were separated on 4.5% SDS PAGE gels and transferred to nitrocellulose membranes, which were incubated overnight at 4°C with primary antibodies, washed and incubated for 2 h at room temperature with the corresponding HRP-conjugated secondary antibodies (Jackson ImmunoResearch). Immunostaining was visualized by ECL (GE Healthcare).

Accession numbers. The sequences of mouse 480AnkG and 270AnkG cDNAs have been submitted to the EMBL with the WEBIN ID number HG915716 and HG915715, respectively.

Results

The tail domain of 480 kDa ankyrin-G mediates its specific interaction with microtubules in an EB-dependent manner

EBs were shown to interact with AnkG in mature neurons (Leterrier et al., 2011). We used computational analysis to characterize the precise EB-binding sites in the three AnkG splice isoforms (190, 270, and 480 kDa; Fig. 1*A*), and identified 12 SxIP motifs in the mouse AnkG sequence. Notably, 10 SxIP motifs were located in the alternatively spliced giant exon encoding the tail domain of 480AnkG isoform and nine of them were conserved in its human orthologue (Fig. 1*A*,*B*). Furthermore, four of the SxIP motifs in the tail domain were repeated in tandem, which was shown to increase the affinity for EB1 (Honnappa et al., 2009). We next overexpressed GFP-tagged version of the three AnkG splice isoforms in COS-7 cells and analyzed their colocalization with EBs on MT plus ends. Only 480AnkG-GFP showed a striking comet-like distribution, appeared at the end of dynamic tyrosinated MTs (Fig. 1*C*, arrows) and strongly colocalized with endogenous EB1 (Fig. 1*D*, arrows). Live cell imaging showed that 480AnkG-GFP comets were highly motile with a growth rate of 0.55 ± 0.02 μm/s (quantified in Fig. 1*E*), which is reminiscent of growing MTs in COS-7 cells. The ability of 480AnkG to associate with growing MT ends was further confirmed by simultaneous dual color live imaging of 480AnkG-GFP and EB3-RFP: 480AnkG tracks the same MT plus ends as EB3 (Fig. 1*F*–*H*). In contrast, 270AnkG-GFP, which was initially shown to interact with EBs in mature neurons (Leterrier et al., 2011), and 190AnkG-GFP were diffusely expressed in the cytoplasm and did not display any comet-like pattern (Fig. 1*C*,*D*). To assess the role of the SxIP-rich tail domain in the selective targeting of 480AnkG to MT plus ends, we overexpressed a GFP-tagged tail domain (480Tail-GFP) or a mutated form of full-length 480AnkG-GFP, in which the 10 SxIP motifs of the tail domain were mutated in SxNN (480AnkG-NN-GFP). Strikingly, 480Tail-GFP showed a highly similar comet-like distribution and behavior to those of full-length 480AnkG (Fig. 1*C*,*D*) and strongly colocalized with endogenous EB1 (Fig. 1*D*, arrows). In contrast, 480AnkG-NN-GFP did not reveal any comet-like pattern or MT plus-end movements, and appeared diffuse in the cytoplasm (Fig. 1*C*,*D*), indicating that the comet-like distribution depends on the EB binding motifs in 480AnkG tail domain. Remarkably, 480AnkG-GFP also showed a comet-like distribution within the soma and neurites of unpolarized cultured hippocampal neurons before AIS formation at DIV1, and strongly overlaps with endogenous EB1 (Fig. 1*I*, arrows in the zooms). Consistently, expression of 480AnkG-NN-GFP in unpolarized neurons only revealed a diffuse signal in the cytoplasm (Fig. 1*I*). Together, our data indicate that, like other EB-binding partners (Jiang et al., 2012), 480AnkG may behave as a +TIP, whereas the other two AnkG isoforms of 270 and 190 kDa fail to colocalize with +TIP core proteins, in contrast to what has been published for 270AnkG (Leterrier et al., 2011).

Depletion of 480 kDa ankyrin-G impairs AIS assembly and neuronal polarity

To investigate the role of 480AnkG in the AIS assembly, we first analyzed the expression pattern of this AnkG longest isoform in mouse embryonic and adult spinal cord and hippocampus using 480AnkG-specific antibody. The 480AnkG antibody was raised against its tail domain (Fig. 2*A*), and reacted strongly and specif-

←

(*Figure legend continued.*) DIV8 neurons cotransfected at DIV1 with GFP and control (white bars), or 480AnkG-shRNA (gray bars) showing 480AnkG, Pan(SR)AnkG, or Pan(SBD)AnkG staining at the AIS (at least 60 neurons were analyzed per condition). ***K***, DIV5 mouse hippocampal neurons cotransfected at DIV1 with GFP (green) and control- or 480AnkG-shRNA and stained with 480AnkG (red) or Pan(SR)AnkG (red) and Pan(SBD)AnkG (gray) antibodies. Right, Top, Higher-magnifications of the boxed regions in the left panels. ***L***, Mean fluorescence intensity profile of 480AnkG, Pan(SR)AnkG and Pan(SBD)AnkG staining along the axon of untransfected neurons (gray line; $n = 7$, 7, and 6, respectively) and along the longest neurite of neurons coexpressing GFP and 480AnkG-shRNA (black line; $n = 7$, 7, and 6, respectively). ***F***, ***G***, ***J***, ***L***, Error bars represent SEM. ***D***, ***E***, ***K***, Arrowheads point to the AIS, whereas arrows indicate the longest neurite, and the open arrowhead highlights the AIS of a non-transfected neuron. Scale bars: ***K*** (top, left), 30 μm; all other panels, 15 μm.

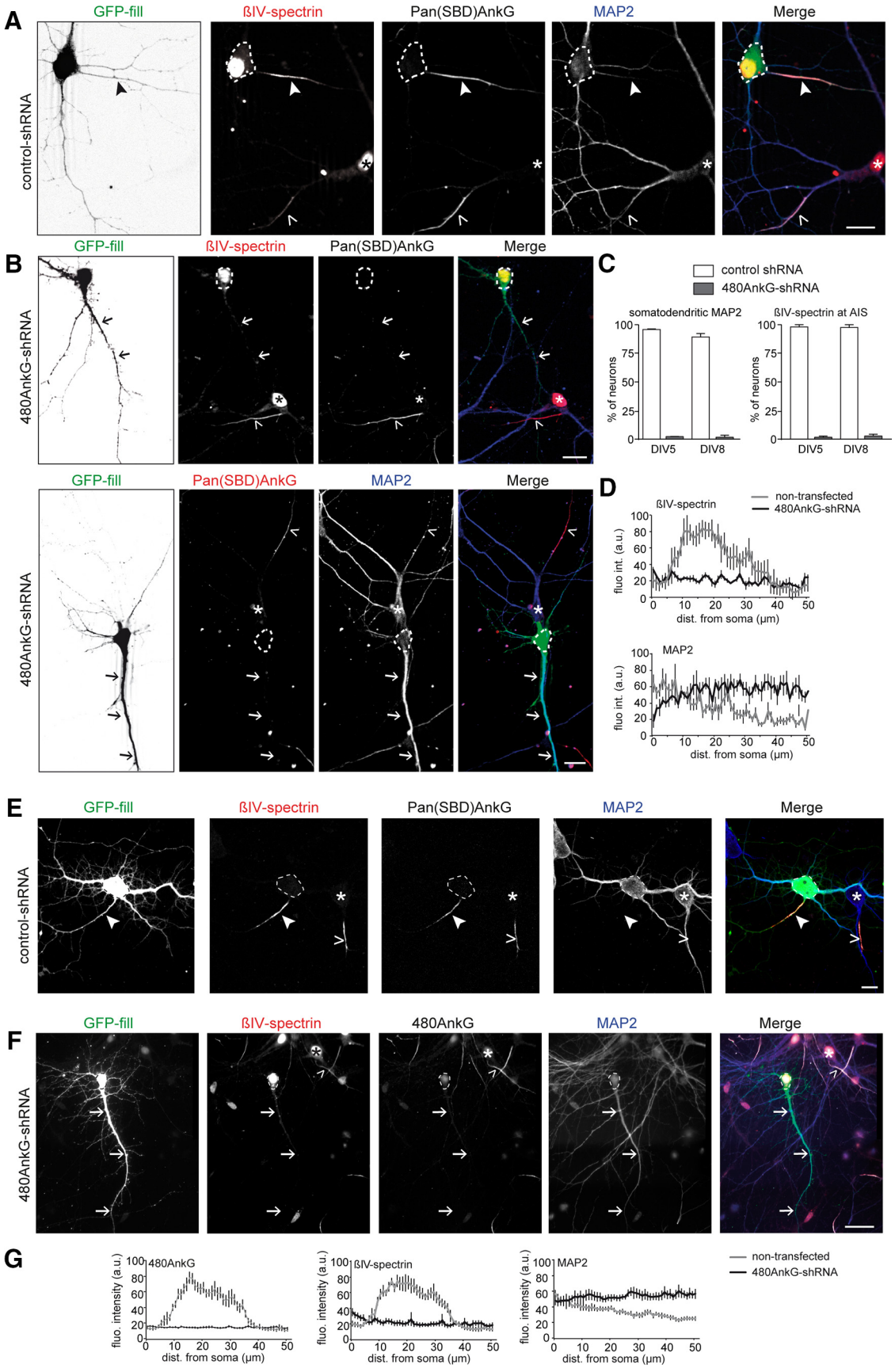

Figure 3. 480AnkG is required for the AIS formation and the maintenance of axonal identity. ***A***, DIV5 mouse hippocampal neurons cotransfected at DIV1 with GFP (green) and control-shRNA and stained for βIV-spectrin (red), Pan(SBD)AnkG (gray), and MAP2 (blue). ***B***, DIV5 mouse hippocampal neurons cotransfected at DIV1 with GFP (green) and 480AnkG-shRNA and stained for βIV-spectrin (red) and Pan(SBD)AnkG (gray) or Pan(SBD)AnkG (red) and MAP2 (blue). ***C***, Average percentage of DIV5 or DIV8 mouse neurons cotransfected at DIV1 with (*Figure legend continues.*)

ically with 480AnkG on Western blot (Fig. 2*B*,*C*). 480AnkG was expressed at early stages of mouse embryonic development and specifically localized to the AIS (Fig. 2*D*,*E*). Western blot analysis of 480/270AnkG ratio in embryonic tissues and cultured neurons showed that the expression of these isoforms varied over time and revealed an enrichment of 480AnkG at the stages of AIS formation (E10.5–E15.5 in the spinal cord and DIV3–DIV5 in cultured neurons; Fig. 2*F*,*G*, 480AnkG-specific bands are indicated by brackets). Furthermore, we confirmed the specificity of our 480AnkG antibody in a heterologous cell system, where it selectively recognized 480AnkG-GFP but neither 190- nor 270AnkG-GFP constructs when expressed in COS7 cells (Fig. 2*H*). Altogether, these results suggest that 480AnkG is the major isoform expressed during early neuronal development both *in vitro* and *in vivo*.

We next designed shRNAs to selectively knockdown 480 AnkG expression (480AnkG-shRNA) in cultured embryonic hippocampal neurons. Because AnkG has a long half-life (Hedstrom et al., 2007), we transfected the 480AnkG-shRNA in DIV1 neurons to rapidly downregulate its expression level. The transfection of 480AnkG-shRNA specifically depleted 480AnkG isoform (Fig. 2*I*, bracket) and strongly reduced 480AnkG and PanAnkG staining in hippocampal neurons (Fig. 2*J–L*, arrows), in contrast to untransfected and control-shRNA transfected neurons (Fig. 2*K*, arrowhead). The 480AnkG-shRNA also abolished the clustering of the AnkG binding partner βIV-spectrin in ~95% of DIV5–DIV8 neurons (Fig. 3*A–G*; *B*,*F*, arrows). Moreover, the knockdown of 480AnkG disrupted proximal axon polarity because the somatodendritic marker MAP2 mislocalized to the axon in ~98% of 480AnkG-depleted DIV5–DIV8 neurons (Fig. 3*A–G*; *B*,*F*, arrows). The presence of MAP2 in the proximal axon has previously been described for panAnkG-depleted neurons (Hedstrom et al., 2007; Sobotzik et al., 2009). This phenotype is still observed in DIV8 480AnkG-depleted neurons (Fig. 3*E–G*), indicating that the loss of 480AnkG did not delay but completely prevented building of the proximal axon. Consistent with recent data (Jenkins et al., 2015), these results show that 480AnkG is required for AIS assembly and proximal axodendritic polarity.

Depletion of 480 kDa ankyrin-G impairs EB accumulation and microtubule orientation in the proximal axon

Although EB proteins are usually associated with growing MT plus ends, they have been described to accumulate along the MT lattice in the proximal axon (Nakata and Hirokawa, 2003). Endogenous EBs indeed concentrate in the proximal axon of developing neurons where they partially colocalize with 480AnkG from DIV2 onward (Fig. 4*A–C*; *A*, arrowheads). We next investigated whether 480AnkG was required for EB localization and global MT organization in the proximal axon. Notably, the accumulation of endogenous EB1 at the AIS of control neurons (Fig. 4*D*,*G*, arrowheads) was lost in ~95% of the 480AnkG-depleted neurons (Fig. 4*D*,*E*, arrows) and the overall EB1 intensity in the soma was significantly reduced in these neurons (Fig. 4*F*) compared with control neurons (Fig. 4*D–I*). Moreover, the vast amount of stationary EB3-GFP at the AIS of control neurons (Fig. 4*J–K*, arrowheads; *J*, vertical black lines on kymographs) was strikingly reduced in the proximal region of 480AnkG-depleted axons (Fig. 4*J–L*), suggesting a role for 480AnkG in the stabilization of EBs at the AIS. Furthermore, the polarized orientation of growing MT plus ends was slightly altered in 480AnkG-shRNA-expressing neurons (Fig. 4*M*). Kymograph analysis of EB3-GFP movements revealed that 480AnkG knockdown in neurons led to a similar proportion of retrograde comets in all neurites to that observed for the dendrites of control neurons. These results are consistent with the neuronal polarity defect of 480AnkG-depleted neurons (Fig. 3*A–G*).

To determine whether 480AnkG stabilizes EBs in specific cellular compartments, we moved back to COS-7 cells, in which we artificially targeted wild-type and EB-binding-deficient 480AnkG-GFP (480AnkG-NN-GFP) to the plasma membrane by coexpressing a membrane AnkG binding partner, Kv-Nav, and analyzed the endogenous EB1 distribution (Fig. 4*N*,*O*). Unlike membrane-targeted 480AnkG-NN-GFP, 480AnkG-GFP induced a strong local recruitment of EBs at the cell cortex (Fig. 4*N*, arrowheads). EB1 was specifically enriched in 480AnkG-GFP-positive patches at the plasma membrane (Fig. 4*N*,*O*). Altogether, these data suggest a role for 480AnkG in organizing the characteristic MT network at the proximal axon during early neuronal development.

EB binding is required for 480 kDa ankyrin-G restricted localization and stabilization at the AIS

We next determined the role of EBs in 480AnkG-mediated AIS formation. We first verified the efficiency of the EB1/3 knockdown with EB-shRNA (Komarova et al., 2005; Jaworski et al., 2009), which indeed led to a significant decrease in EB1 signal and a markedly reduced number of EB1 comets in transfected neurons compared with control neurons (Fig. 5*A–C*). In EB-shRNA-expressing neurons, the endogenous 480AnkG staining was significantly reduced in the proximal axon (Fig. 5*D–F*; *E*, arrowheads) and abnormally detected in multiple Tau-1-negative neurites (Fig. 5*E*, arrows in enlargements) in the majority of EB-depleted neurons (Fig. 5*G*). Similar effects were observed by coexpressing 480AnkG-GFP with EB-shRNA: 480AnkG-GFP was no longer restricted to the proximal axon and mislocalized to multiple processes in the absence of EBs (Fig. 5*H–L*; *H*, arrows). This missorting of 480AnkG in EB-depleted neurons was tightly correlated with an ectopic expression of Nav in the majority of EB-depleted neurons (Fig. 5*H–J*), but without a significant decrease of Nav staining at the AIS (Fig. 5*I*). These findings indicate that EBs are required to restrict 480AnkG localization at the AIS. It will be interesting to further explore the nature of the Tau-negative and AnkG/Nav-positive neurites.

We next tested whether EBs could stabilize 480AnkG-GFP at the AIS by performing FRAP experiments in neurons depleted of endogenous AnkG. EB-binding-deficient 480AnkG (480AnkG-NN-GFP) showed an increased recovery rate (~57%) after photobleaching compared with the wild-type isoform (~24%;

←

(*Figure legend continued.*) GFP and control- (white bars) or 480AnkG-shRNA (gray bars) showing the somatodendritic restriction of MAP2 and the accumulation of βIV-spectrin at the AIS (at least 60 neurons were analyzed per condition). ***D***, Mean fluorescence intensity profile of βIV-spectrin and MAP2 along the axons of untransfected neurons (gray line; $n = 6$ and 5, respectively) and along the longest neurite of neurons coexpressing GFP and 480AnkG-shRNA (black line; $n = 6$ and 5, respectively). ***E***, DIV8 mouse hippocampal neurons cotransfected at DIV1 with GFP (green) and control-shRNA and stained for βIV-spectrin (rabbit antibody, red) and Pan(SBD)AnkG (gray). ***F***, DIV8 mouse hippocampal neurons cotransfected at DIV 1 with GFP (green) and 480AnkG-shRNA and stained for βIV-spectrin (chicken antibody, red), 480AnkG (gray) and MAP2 (blue). ***G***, Mean fluorescence intensity profile of 480AnkG, βIV-spectrin and MAP2 along the axons of DIV8 untransfected neurons (gray line; $n = 5$ for each condition) and along the longest neurite of neurons cotransfected with GFP and 480AnkG-shRNA (black line; $n = 5$ for each condition). ***A***, ***B***, ***E***, ***F***, Arrowheads and open arrowheads point to the AIS of transfected and nontransfected neurons respectively. Arrows indicate the longest neurite of transfected neurons. Dashed lines delineate the cell body of transfected neurons, whereas asterisks pinpoint the soma of untransfected neurons. Scale bars: ***F***, 30 μm; all other panels, 15 μm. Errors bars are SEM.

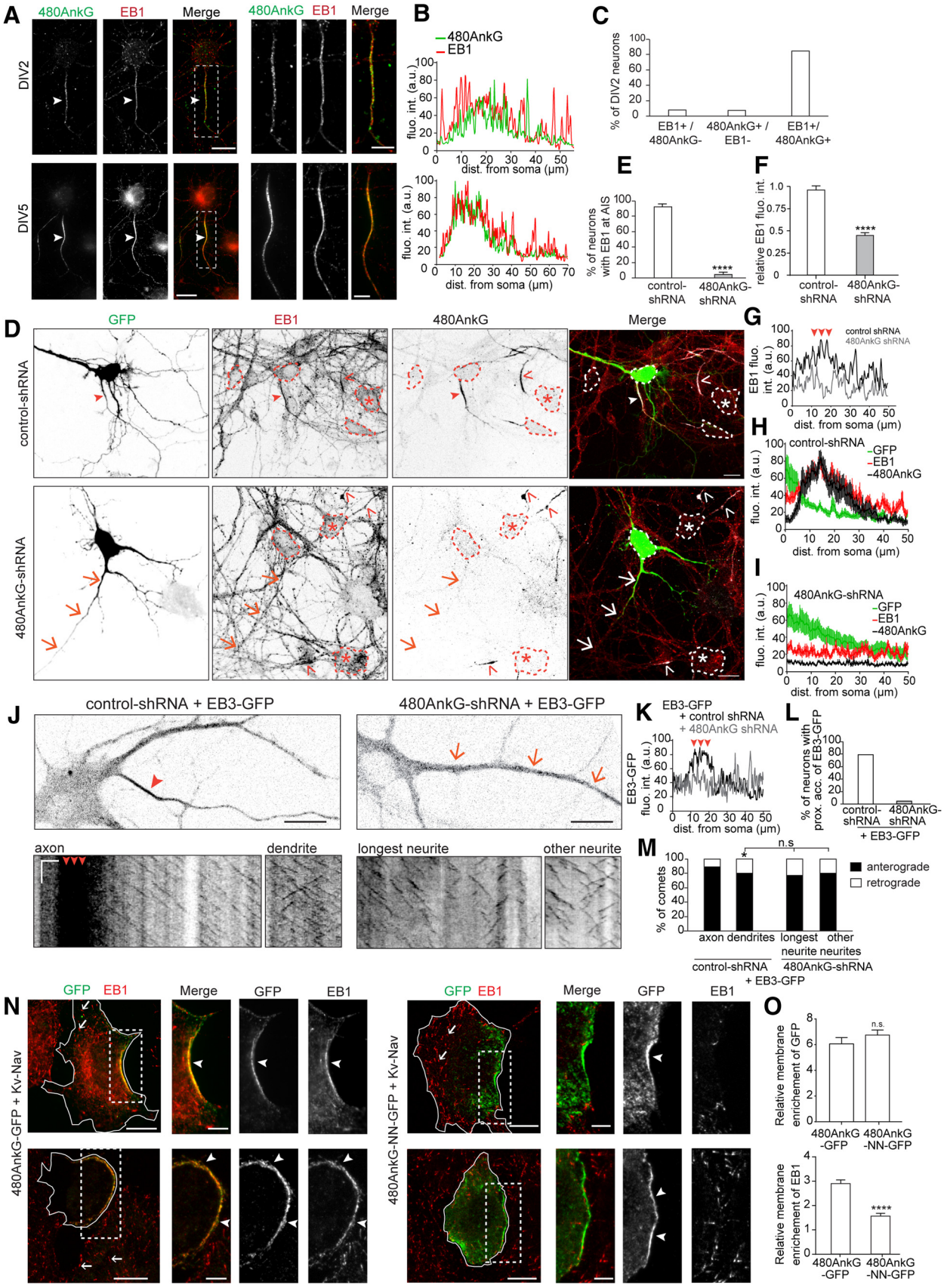

Figure 4. 480AnkG controls EB accumulation and MT polarity orientation in the proximal axon. ***A***, ***B***, Staining of 480AnkG (green) and EB1 (red) in rat DIV2 (top) and DIV5 (bottom) hippocampal neurons (***A***) and corresponding fluorescence intensity profile along their axons (***B***). Arrowheads point to the proximal accumulation of 480AnkG and EB1. ***C***, Percentage of DIV2 neurons showing an accumulation of EB1 and/or 480AnkG in their proximal axon. $n = 189$ neurons. ***D***, DIV5 rat hippocampal neuron cotransfected at DIV1 with GFP (green) and control, (top) or 480AnkG-shRNA (bottom) and stained for EB1 (red) and 480AnkG (gray). Arrowheads highlight the AIS, whereas arrows indicate the longest neurite of transfected neurons. Asterisks (*Figure legend continues.*)

Fig. 5*M–O*), showing that the interaction with EBs stabilizes 480AnkG at the AIS.

The interaction between 480 kDa ankyrin-G and EBs drives AIS formation and neuronal polarity

To further assess the functional relevance of 480AnkG interaction with EBs, we tested the ability of 480AnkG-GFP, 480AnkG-NN-GFP, or 270AnkG-GFP to rescue the AIS and polarity defects associated with total AnkG depletion (Hedstrom et al., 2007, 2008). Silencing of all endogenous AnkG isoforms was performed in DIV0 rat embryonic hippocampal neurons with the selective rat AnkG-shRNA (Hedstrom et al., 2007; Fig. 6*A–I*), which did not alter the expression of mouse exogenous GFP-tagged AnkG constructs in rescue experiments (Fig. 6*J*) and abolished PanAnkG immunostaining in ~85% of DIV5 transfected neurons (data not shown). PanAnkG-depleted neurons showed both AIS and polarity defects characterized by the lack of the main AIS markers including Nfasc, Nav, and βIV-spectrin, as well as the abnormal entry of MAP2 in the axon. PanAnkG-depleted neurons expressing 480AnkG-GFP (Fig. 6*A*,*B*) were undistinguishable from control neurons cotransfected with 480AnkG-GFP and control-shRNA (Fig. 5*H*, top). In neurons cotransfected with rat AnkG-shRNA and mouse 480AnkG-GFP, the exogenous 480AnkG was correctly restricted to the AIS in >60% of the neurons (Fig. 6*A*,*B*,*G*,*H*), where it recruited the AIS proteins Nfasc and Nav (Fig. 6*A*,*B*,*G*; *A*, arrowheads), whereas MAP2 showed its proper somatodendritic distribution (Fig. 6*A*,*I*). In contrast, 480AnkG-NN-GFP was not restricted to the AIS in ~80% of the neurons in the absence of endogenous AnkG and mislocalized to the whole neuron (Fig. 6*C*,*D*,*H*), which further emphasized the critical role of the interaction with EBs for the accumulation of 480AnkG at the AIS. Moreover, the expression of 480AnkG-NN-GFP in PanAnkG-depleted neurons failed to rescue the clustering of Nfasc or Nav (Fig. 6*C*,*D*,*G*; *C*, arrows) and the aberrant localization of MAP2 in the axon (Fig. 6*C*,*I*). Consistently, 270AnkG-GFP did not cluster at the AIS of PanAnkG-depleted neurons (Fig. 6*H*), appeared diffuse throughout the whole neuron (Fig. 6*E*,*F*,*H*), and did not rescue NFasc nor Nav clustering (Fig. 6 *E–G*; *E*, arrows) and polarity defects (Fig. 6*E*,*I*). Altogether, our data thus point out the strong cooperative relationship between the characteristic organization of MTs in the proximal axon and the formation of AnkG-mediated AIS architecture.

Discussion

Although 480AnkG was recently defined as the master-organizer of the AIS, the specific characteristics of this longest AnkG isoform, conferring its key role in AIS assembly and neuronal polarity, remained elusive. In this study, our functional analysis revealed a unique property of the 480AnkG isoform: the tail domain of 480AnkG binds to EBs and is required for proper axonal MT organization and AIS formation. We thus propose a model in which AnkG promotes AIS assembly via a cooperative interaction with EBs in the proximal axon. It is very likely that the cooperative binding between 480AnkG and EBs drives the self-organized assembly of the MT-AIS structure during neuronal development, which subsequently promotes compartmentalization of the proximal axon and mediates further axon specification and neuronal polarity. Self-assembly of diverse cytoskeleton-based structures occurs in a wide variety of other cellular processes and is essential for many basic cellular functions, such as mitosis, organelle positioning, and cell polarity (Subramanian and Kapoor, 2012; Abu Shah and Keren, 2013).

480 kDa ankyrin-G is required for AIS assembly and neuronal polarity

Until recently, the role of AnkG in the AIS assembly had been investigated by eliminating all AnkG isoforms together (for review, see Rasband, 2010), but a growing number of functional studies lately revealed differential roles for each AnkG isoform in neuronal physiology. Furthermore, the three neuronal AnkG isoforms show distinct fine-tuned expression patterns in both space and time, which highlights the relevance of deciphering the specific roles of AnkG isoforms in neuronal development and functioning. Notably, the levels of human 270AnkG- and 480AnkG-encoding transcripts significantly vary across brain structures and throughout embryogenesis (Rueckert et al., 2013). Here we show that the levels of mouse 480AnkG are higher than those of 270AnkG at the developmental stages of AIS formation. AnkG isoforms often form nanodomains within neurons; for example, 190AnkG specifically localizes to dendritic spines where it regulates spine structure and function (Smith et al., 2014), whereas the giant 480AnkG was shown to accumulate at both the AIS and the nodes of Ranvier where it plays a pivotal role in the establishment and maintenance of neuronal polarity (Jenkins et al., 2015; present study). In mature neurons, 480AnkG is also observed at the soma surface and in the dendritic shafts, where it promotes GABAergic synapse stability (Tseng et al., 2015). In contrast, less is known about the role of 270AnkG isoform at the AIS where it was shown to accumulate after overexpression in wild-type neurons (Zhang and Bennett, 1998). Our rescue analysis shows that 270AnkG fails to localize on its own in the proximal axon and to build the AIS in the absence of 480AnkG isoform, which demonstrates its secondary role in the AIS assembly. Overall, the combined data on the comparative function of 480AnkG/270AnkG suggest that 480AnkG most likely recruits

←

(*Figure legend continued.*) and open arrowheads pinpoint the soma and the AIS of nontransfected neurons respectively. Dashed lines delimit cell bodies. ***E***, ***F***, Percentage of neurons with an accumulation of EB1 at AIS (***E***) and EB1 fluorescence intensity ratio (***F***) in the soma of neurons cotransfected at DIV1 with GFP and a control, (white bars; $n = 41$ in ***E*** and 35 in ***F***) or a 480AnkG-shRNA (gray bars; $n = 50$ in ***E*** and 37 in ***F***) normalized to neighboring nontransfected neurons. Unpaired *t* test, $p = 4.95 \times 10^{-5}$ in ***E*** and 1.01×10^{-14} in ***F***. ***G***, Fluorescence intensity profile of endogenous EB1 along the axon (black line) and longest neurite (gray line) of the neuron transfected with control (***D***, top) and 480AnkG-shRNA (***D***, bottom). Arrowheads show the position of the AIS. ***H***, ***I***, Mean fluorescence intensity profile of GFP, EB1, and 480AnkG along the axon (***H***) or the longest neurites (***I***) of neurons cotransfected with GFP and a control, (***H***) or 480AnkG-shRNA (***I***). $n = 9$ neurons per condition. ***J***, Representative stills (***J***, top) and kymographs (***J***, bottom) from a time-lapse recording of mouse DIV5–DIV6 hippocampal neurons cotransfected with EB3-GFP and control (left), or 480AnkG-shRNA (right) and corresponding fluorescence intensity profile (***K***) along the axon (black line) or the longest neurite (gray line) of the control (***J***, left) or the 480AnkG-depleted neurons (***J***, right). Vertical and horizontal bars represent 60 s and 5 μm, respectively. Arrowheads highlight the position of the AIS, whereas arrows show the longest neurite of transfected neurons. ***L***, Percentage of DIV5–DIV6 neurons transfected with EB3-GFP and control, ($n = 24$) or 480AnkG-shRNA ($n = 18$) showing an accumulation of GFP in the proximal axon. ***M***, Percentage of anterogradely (black bars) and retrogradely moving (white bars) comets in the proximal axon ($n = 18$) versus the proximal dendrites ($n = 100$) of DIV5–DIV6 neurons cotransfected with EB3-GFP and control-shRNA, or in the longest ($n = 18$) versus other neurites ($n = 67$) of neurons coexpressing EB3-GFP and 480AnkG-shRNA. ANOVA, $^{*}p = 0.044$. ***N***, COS-7 cells cotransfected with Kv-Nav and 480AnkG-GFP (left) or 480AnkG-NN-GFP (right) and stained for GFP (green) and EB1 (red). ***O***, Mean fluorescence intensity ratio of GFP (top) and EB1 (bottom) staining within membrane patches versus the rest of the cell, in COS-7 cells expressing Kv-Nav together with 480AnkG-GFP ($n = 39$) or 480AnkG-NN-GFP ($n = 53$). Unpaired *t* test; top, $p = 0.276$; bottom, $p = 5.87 \times 10^{-9}$. Arrowheads and arrows indicate EB accumulation and MT plus ends, respectively. A.U., Arbitrary units. n.s., nonsignificant. Scale bars: ***A***, ***D***, ***N***, 15 μm; ***A***, ***D***, ***N*** (zoomed), 5 μm. Error bars are SEM. $^{*}p < 0.05$; $^{****}p < 0.0001$.

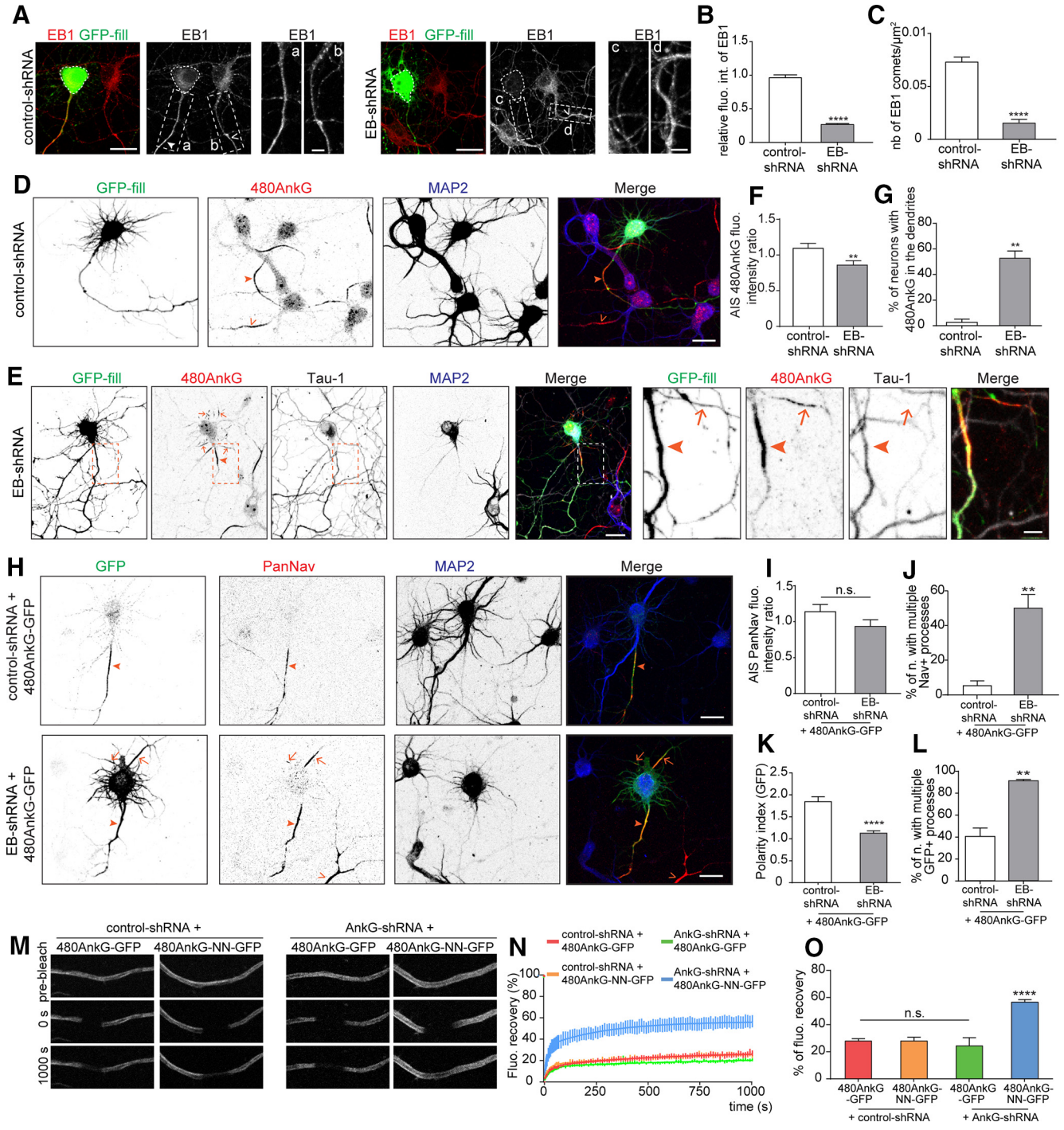

Figure 5. Interaction of 480AnkG with EBs is critical for its restricted localization and stabilization at the AIS. ***A***, DIV5 rat neurons cotransfected with GFP and control- or EB-shRNA and stained for GFP (green) and EB1 (red). Enlargement of the boxed areas are shown for transfected (a, c) and nontransfected (b, d) neurons. The soma of transfected neurons is delimited by dashed lines. ***B***, ***C***, EB1 fluorescence intensity ratio (***B***) and mean number of EB1 comets per micrometer squared (***C***) in the soma of neurons cotransfected at DIV1 with GFP and control- (white bars) or EB-shRNA (gray bars). ***B***, Mann–Whitney test, $n = 26$ neurons at least per condition $p = 4.03 \times 10^{-5}$. ***C***, Unpaired *t* test, $n = 32$ neurons at least per condition, $p = 7.79 \times 10^{-15}$. ***D***, ***E***, DIV5 rat neurons cotransfected at DIV1 with GFP and control- (***D***) or EB-shRNA (***E***) and stained for GFP (green), 480AnkG (red), MAP2 (blue), and Tau-1 (***E***, gray). ***E***, Right, Enlargements of the left panel boxed areas. ***F***, Fluorescence intensity of 480AnkG staining at the AIS of DIV5 neurons cotransfected at DIV1 with GFP and control- ($n = 34$) or EB-shRNA ($n = 26$), normalized to neighboring untransfected neurons. Unpaired *t* test, $p = 0.0094$. ***G***, Percentage of DIV5 neurons cotransfected at DIV1 with GFP and control- ($n = 94$) or EB-shRNA ($n = 92$) showing endogenous 480AnkG in dendrites. Unpaired *t* test, $p = 0.0013$. ***H***, DIV5 hippocampal neurons cotransfected at DIV1 with 480AnkG-GFP (green) and control- (top) or EB-shRNA (bottom) and stained for PanNav (red) and MAP2 (blue). ***I***, Fluorescence intensity of PanNav staining at the AIS of DIV5 neurons transfected with 480AnkG-GFP and control- ($n = 21$) or EB-shRNA ($n = 24$) normalized to neighboring untransfected neurons. Unpaired *t* test, $p = 0.14$. ***J***, Percentage of DIV5 neurons cotransfected with 480AnkG-GFP and control- ($n = 53$) or EB-shRNA ($n = 47$) showing PanNav immunoreactivity in dendrites. Unpaired *t* test, $p = 0.0059$. ***K***, Polarity index of GFP in DIV5 neurons coexpressing 480AnkG-GFP together with control- ($n = 21$) or EB-shRNA ($n = 23$). Mann–Whitney test, $p = 7.00 \times 10^{-7}$. ***L***, Average percentage of DIV5 neurons transfected with 480AnkG-GFP and control- ($n = 97$) or EB-shRNA ($n = 76$) showing a dendritic localization of GFP. Unpaired *t* test, $p = 0.029$. ***M–O***, FRAP experiments in the proximal axon of DIV5–DIV6 hippocampal neurons cotransfected at DIV0 with 480AnkG-GFP or 480AnkG-NN-GFP and control-shRNA or AnkG-shRNA. Representative stills of corresponding time-lapse videomicroscopy recording (***M***), percentage of GFP fluorescence recovery after FRAP (***N***), and percentage of normalized GFP fluorescence recovery (***O***), at least 10 neurons per condition were analyzed. One-way ANOVA. Arrowheads and empty arrowheads indicate the AIS of transfected and nontransfected neurons respectively. Arrows highlight the ectopic localization of AIS components. Scale bars, 20 μm and 5 μm in the zooms (***A***, ***E***). Error bars are SEM. n.s., Nonsignificant. $^{**}p < 0.01$, $^{****}p < 0.0001$.

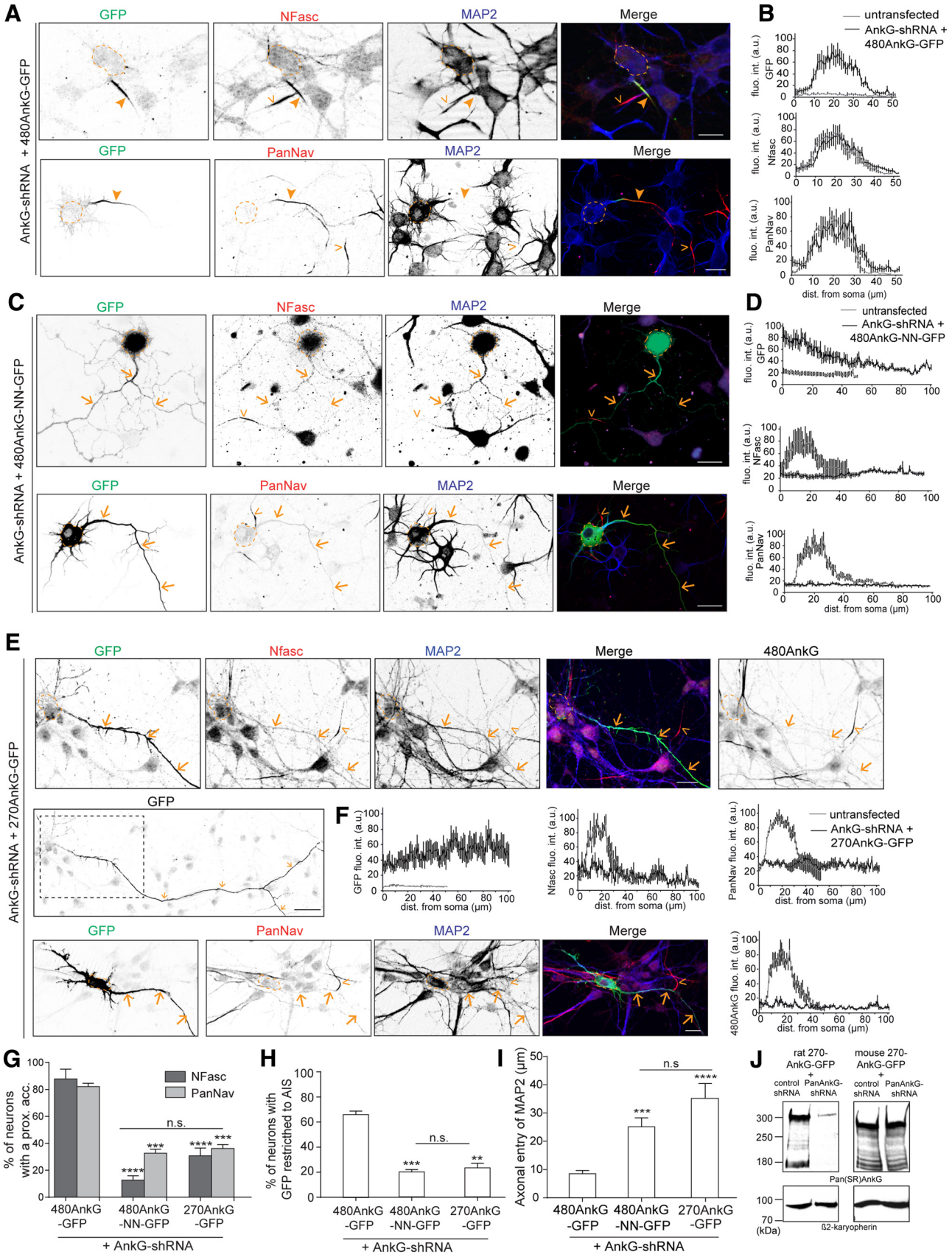

Figure 6. 480AnkG exclusively orchestrates AIS assembly through its interaction with EBs. ***A***, DIV5 rat hippocampal neurons cotransfected at DIV0 with AnkG-shRNA and 480AnkG-GFP (green) and stained for Nfasc (top, red) or PanNav (bottom, red), and MAP2 (blue). ***B***, Mean fluorescence intensity profile of GFP, NFasc and PanNav staining along the axons of untransfected neurons (gray lines) and neurons coexpressing AnkG-shRNA and 480AnkG-GFP (black lines, at least 7 neurons per condition). ***C***, DIV5 rat hippocampal neurons cotransfected at DIV0 with AnkG-shRNA and 480AnkG-NN-GFP (green), and stained for Nfasc (top, red) or PanNav (bottom, red) and MAP2 (blue). ***D***, Mean fluorescence intensity profile of GFP, NFasc, and (*Figure legend continues.*)

the abundant 270AnkG isoform at the AIS to consolidate its architecture by locally increasing the number of binding sites for the recruitment of AIS membrane components, like voltage-gated channels and βIV-spectrin. We thus demonstrate that 480AnkG is unique because it is the only isoform that associates with EBs.

Interaction of 480AnkG with EBs is crucial for AIS assembly and neuronal polarity

Our results indicate that the cooperative interactions between 480AnkG and EB proteins assemble the axon initial segment. At the AIS, EBs accumulate as a stable pool along the MT lattice and are not specifically localized to MT plus-ends (Nakata and Hirokawa, 2003; Leterrier et al., 2011). This unusual EB distribution is most likely required for local anchoring and selective stabilization of 480AnkG at the AIS. Because MTs at the AIS are remarkably stable (Gomis-Rüth et al., 2008; Konishi and Setou, 2009; Sanchez-Ponce et al., 2011), the interaction between 480AnkG and EBs may even contribute to local MT stabilization. The EB stretches at the AIS may increase MT stability by direct binding to the MT polymer and/or acting as local membrane-MT anchoring sites (Iwakura et al., 2012; Le Bras et al., 2014). Our analysis revealed that submembranous 480AnkG accumulates EBs and can act as cortical anchors to locally stabilize MTs. This phenomenon is very similar to what has been reported for the ER-transmembrane protein STIM1 (Grigoriev et al., 2008) and the membrane-bound plus-end binding proteins, APC and CLASPs (Etienne-Manneville et al., 2005; Lansbergen et al., 2006). Furthermore, 480AnkG may not only affect MT stability but also influence local MT organization. Characteristic MT bundles are described as the structural hallmark of the AIS (Palay et al., 1968) and this typical MT organization recently emerged as an early event in AIS formation (Jones et al., 2014). This distinctive MT bundling is absent from the axon of mouse total AnkG- or specific giant exon-null neurons (Sobotzik et al., 2009; Jenkins et al., 2015). Our analysis showed that 480AnkG-depleted neurons also displayed an abnormal "dendritic-like" anti-parallel MT orientation in their proximal axon. How these two different MT phenotypes of 480AnkG-depleted neurons relate to each other remains to be determined. Although MT polarity patterns control motor-driven transport and hence indirectly trigger cell polarity through the asymmetric distribution of organelles and proteins in the cytoplasm (Kapitein and Hoogenraad, 2011), the precise role of MT organization in neuronal polarity is still debated (Baas and Lin, 2011). Interestingly, MT organization, orientation and post-translational modifications were shown to provide directional information for polarized axon transport via the selective affinity of molecular motors for different MT subpopulations: for example, the axonal motor kinesin-1 shows a significant preference for the MTs of the AIS (Nakata and Hirokawa, 2003). We hypothesize that the observed dendritic-like orientation of MTs in 480AnkG-depleted proximal axons could have an impact on the polarized axonal transport. However, the complete loss of all known AIS components in AnkG giant exon-null neurons did not reveal major changes in axonal lysosome trafficking and the polarized localization of transferrin receptor (Jenkins et al., 2015). These data combined with our findings either suggest that AIS-independent mechanisms are responsible for the selective sorting of polarized cargos, or that only a subset of molecular motors (Brown et al., 2005; Loubéry et al., 2008), and may be not those moving lysosomes, is controlled by the specific MT organization at the AIS. It is even possible that redundant motors take over some of the axon and dendritic cargo trafficking pathways in AIS-depleted cells.

Unraveling the specific localization and physiological functions of AnkG isoforms is of utmost importance, particularly, because the human AnkG-encoding gene, *ANK3*, has lately been identified as a risk locus for different bipolar disorders (for review, see Harrison, 2015). Interestingly a frame-shift mutation specifically targeting 480AnkG is associated with intellectual disability, hyperactivity and attention deficit disorder (Iqbal et al., 2013), which further support the physiological importance of 480AnkG during neuronal development. Further characterization of the differential roles played by each AnkG isoform will permit to decipher their possibly distinct involvement in the pathogenicity of various neurodevelopmental and psychiatric disorders, such as intellectual disability, schizophrenia, or other bipolar disorders.

←

(*Figure legend continued.*) PanNav staining along the axon of untransfected neurons (gray lines) and along the longest neurite of neurons coexpressing AnkG-shRNA and 480AnkG-NN-GFP (black lines, at least 7 neurons per condition). ***E***, DIV5 rat hippocampal neurons cotransfected at DIV0 with AnkG-shRNA and 270AnkG-GFP (green), and stained for Nfasc (top, red) or PanNav (bottom, red) together with MAP2 (blue). ***F***, Mean fluorescence intensity profile of GFP, NFasc, PanNav, and 480AnkG along the axon of untransfected neurons (gray lines) and along the longest neurite of neurons coexpressing AnkG-shRNA and 270AnkG-GFP (black lines, at least 6 neurons per condition). ***G***, ***H***, Average percentage of neurons cotransfected with AnkG-shRNA and 480AnkG-GFP ($n = 56$), 480AnkG-NN-GFP ($n = 48$), or 270AnkG-GFP ($n = 81$) showing an accumulation of NFasc (dark gray) or PanNav (light gray) at the AIS (***G***) and GFP staining restricted to the AIS (***H***). One-way ANOVA. ***I***, Distal limit of MAP2 expression in the longest neurite of neurons cotransfected with AnkG-shRNA and 480AnkG-GFP ($n = 16$), 480AnkG-NN-GFP ($n = 13$), or 270AnkG-GFP ($n = 13$). Kruskal–Wallis test. ***J***, Western blot analysis of protein extracts from COS-7 cells cotransfected with control- or AnkG-shRNA and rat or mouse 270AnkG-GFP using Pan(SR)AnkG antibody. β2-karyopherin was used as a loading control. Arrowheads and open arrowheads show the AIS of transfected and nontransfected neurons respectively and arrows point the lack of AIS in transfected neurons. Scale bars: ***A***, ***C***, ***E*** (top), 15 μm; ***E*** (bottom), 30 μm. n.s., Nonsignificant; A.U., arbitrary unit. Error bars represent SEM. $^{**}p < 0.01$, $^{***}p < 0.001$, $^{****}p < 0.0001$.

References

Abu Shah E, Keren K (2013) Mechanical forces and feedbacks in cell motility. Curr Opin cell biol 25:550–557. CrossRef Medline

Baas PW, Lin S (2011) Hooks and comets: the story of microtubule polarity orientation in the neuron. Dev Neurobiol 71:403–418. CrossRef Medline

Bréchet A, Fache MP, Brachet A, Ferracci G, Baude A, Irondelle M, Pereira S, Leterrier C, Dargent B (2008) Protein kinase CK2 contributes to the organization of sodium channels in axonal membranes by regulating their interactions with ankyrin G. J Cell Biol 183:1101–1114. CrossRef Medline

Brown CL, Maier KC, Stauber T, Ginkel LM, Wordeman L, Vernos I, Schroer TA (2005) Kinesin-2 is a motor for late endosomes and lysosomes. Traffic 6:1114–1124. CrossRef Medline

Etienne-Manneville S, Manneville JB, Nicholls S, Ferenczi MA, Hall A (2005) Cdc42 and Par6-PKCzeta regulate the spatially localized association of Dlg1 and APC to control cell polarization. J Cell Biol 170:895–901. CrossRef Medline

Gomis-Rüth S, Wierenga CJ, Bradke F (2008) Plasticity of polarization: changing dendrites into axons in neurons integrated in neuronal circuits. Curr Biol 18:992–1000. CrossRef Medline

Grigoriev I, Gouveia SM, van der Vaart B, Demmers J, Smyth JT, Honnappa S, Splinter D, Steinmetz MO, Putney JW Jr, Hoogenraad CC, Akhmanova A (2008) STIM1 is a MT-plus-end-tracking protein involved in remodeling of the ER. Curr Biol 18:177–182. CrossRef Medline

Gutzmann A, Ergül N, Grossmann R, Schultz C, Wahle P, Engelhardt M (2014) A period of structural plasticity at the axon initial segment in developing visual cortex. Front Neuroanat 8:11. CrossRef Medline

Harrison PJ (2015) Molecular neurobiological clues to the pathogenesis of bipolar disorder. Curr Opin Neurobiol 36:1–6. CrossRef Medline

Hedstrom KL, Xu X, Ogawa Y, Frischknecht R, Seidenbecher CI, Shrager P, Rasband MN (2007) Neurofascin assembles a specialized extracellular

matrix at the axon initial segment. J Cell Biol 178:875–886. CrossRef Medline

Hedstrom KL, Ogawa Y, Rasband MN (2008) AnkyrinG is required for maintenance of the axon initial segment and neuronal polarity. J Cell Biol 183:635–640. CrossRef Medline

Honnappa S, Gouveia SM, Weisbrich A, Damberger FF, Bhavesh NS, Jawhari H, Grigoriev I, van Rijssel FJ, Buey RM, Lawera A, Jelesarov I, Winkler FK, Wüthrich K, Akhmanova A, Steinmetz MO (2009) An EB1-binding motif acts as a microtubule tip localization signal. Cell 138:366–376. CrossRef Medline

Iqbal Z, Vandeweyer G, van der Voet M, Waryah AM, Zahoor MY, Besseling JA, Roca LT, Vulto-van Silfhout AT, Nijhof B, Kramer JM, Van der Aa N, Ansar M, Peeters H, Helsmoortel C, Gilissen C, Vissers LE, Veltman JA, de Brouwer AP, Frank Kooy R, Riazuddin S, et al. (2013) Homozygous and heterozygous disruptions of ANK3: at the crossroads of neurodevelopmental and psychiatric disorders. Hum Mol Genet 22:1960–1970. CrossRef Medline

Iwakura A, Uchigashima M, Miyazaki T, Yamasaki M, Watanabe M (2012) Lack of molecular-anatomical evidence for GABAergic influence on axon initial segment of cerebellar Purkinje cells by the pinceau formation. J Neurosci 32:9438–9448. CrossRef Medline

Jaworski J, Kapitein LC, Gouveia SM, Dortland BR, Wulf PS, Grigoriev I, Camera P, Spangler SA, Di Stefano P, Demmers J, Krugers H, Defilippi P, Akhmanova A, Hoogenraad CC (2009) Dynamic microtubules regulate dendritic spine morphology and synaptic plasticity. Neuron 61:85–100. CrossRef Medline

Jenkins PM, Kim N, Jones SL, Tseng WC, Svitkina TM, Yin HH, Bennett V (2015) Giant ankyrin-G: a critical innovation in vertebrate evolution of fast and integrated neuronal signaling. Proc Natl Acad Sci U S A: 112: 957–964. CrossRef

Jiang K, Toedt G, Montenegro Gouveia S, Davey NE, Hua S, van der Vaart B, Grigoriev I, Larsen J, Pedersen LB, Bezstarosti K,, Lince-Faria M, Demmers J, Steinmetz MO, Gibson TJ, Akhmanova A (2012) A proteome-wide screen for mammalian SxIP motif-containing microtubule plus-end tracking proteins. Curr Biol 22:1800–1807. CrossRef Medline

Jones SL, Korobova F, Svitkina T (2014) Axon initial segment cytoskeleton comprises a multiprotein submembranous coat containing sparse actin filaments. J Cell Biol 205:67–81. CrossRef Medline

Kapitein LC, Hoogenraad CC (2011) Which way to go? Cytoskeletal organization and polarized transport in neurons. Mol Cell Neurosci 46:9–20. CrossRef Medline

Kapitein LC, Hoogenraad CC (2015) Building the neuronal microtubule cytoskeleton. Neuron 87:492–506. CrossRef Medline

Kole MH, Stuart GJ (2012) Signal processing in the axon initial segment. Neuron 73:235–247. CrossRef Medline

Komada M, Soriano P (2002) βIV-spectrin regulates sodium channel clustering through ankyrin-G at axon initial segments and nodes of Ranvier. J Cell Biol 156:337–348. CrossRef Medline

Komarova Y, Lansbergen G, Galjart N, Grosveld F, Borisy GG, Akhmanova A (2005) EB1 and EB3 control CLIP dissociation from the ends of growing microtubules. Mol Biol Cell 16:5334–5345. CrossRef Medline

Konishi Y, Setou M (2009) Tubulin tyrosination navigates the kinesin-1 motor domain to axons. Nat Neurosci 12:559–567. CrossRef Medline

Kordeli E, Lambert S, Bennett V (1995) AnkyrinG: a new ankyrin gene with neural-specific isoforms localized at the axonal initial segment and node of Ranvier. J Biol Chem 270:2352–2359. CrossRef Medline

Lansbergen G, Grigoriev I, Mimori-Kiyosue Y, Ohtsuka T, Higa S, Kitajima I, Demmers J, Galjart N, Houtsmuller AB, Grosveld F, Akhmanova A (2006) CLASPs attach microtubule plus ends to the cell cortex through a complex with LL5β. Dev Cell 11:21–132. CrossRef Medline

Le Bras B, Fréal A, Czarnecki A, Legendre P, Bullier E, Komada M, Brophy PJ, Davenne M, Couraud F (2014) *In vivo* assembly of the axon initial segment in motor neurons. Brain Struct Funct 219:1433–1450. CrossRef Medline

Leterrier C, Vacher H, Fache MP, d'Ortoli SA, Castets F, Autillo-Touati A, Dargent B (2011) End-binding proteins EB3 and EB1 link microtubules to ankyrin G in the axon initial segment. Proc Natl Acad Sci U S A 108: 8826–8831. CrossRef Medline

Loubéry S, Wilhelm C, Hurbain I, Neveu S, Louvard D, Coudrier E (2008) Different microtubule motors move early and late endocytic compartments. Traffic 9:492–509. CrossRef Medline

Nakata T, Hirokawa N (2003) Microtubules provide directional cues for polarized axonal transport through interaction with kinesin motor head. J Cell Biol 162:1045–1055. CrossRef Medline

Palay SL, Sotelo C, Peters A, Orkand PM (1968) The axon hillock and the initial segment. J Cell Biol 38:193–201. CrossRef Medline

Peris L, Thery M, Fauré J, Saoudi Y, Lafanechère L, Chilton JK, Gordon-Weeks P, Galjart N, Bornens M, Wordeman L, Wehland J, Andrieux A, Job D (2006) Tubulin tyrosination is a major factor affecting the recruitment of CAP-Gly proteins at microtubule plus ends. J Cell Biol 174: 839–849. CrossRef Medline

Rasband MN (2010) The axon initial segment and the maintenance of neuronal polarity. Nat Rev Neurosci 11:552–562. CrossRef Medline

Rueckert EH, Barker D, Ruderfer D, Bergen SE, O'Dushlaine C, Luce CJ, Sheridan SD, Theriault KM, Chambert K, Moran J, Purcell SM, Madison JM, Haggarty SJ, Sklar P (2013) Cis-acting regulation of brain-specific ANK3 gene expression by a genetic variant associated with bipolar disorder. Mol Psychiatry 18:922–929. CrossRef Medline

Sanchez-Ponce D, Muñoz A, Garrido JJ (2011) Casein kinase 2 and microtubules control axon initial segment formation. Mol Cell Neurosci 46: 222–234. CrossRef Medline

Smith KR, Kopeikina KJ, Fawcett-Patel JM, Leaderbrand K, Gao R, Schürmann B, Myczek K, Radulovic J, Swanson GT, Penzes P (2014) Psychiatric risk factor ANK3/ankyrin-G nanodomains regulate the structure and function of glutamatergic synapses. Neuron 84:399–415. CrossRef Medline

Sobotzik JM, Sie JM, Politi C, Del Turco D, Bennett V, Deller T, Schultz C (2009) AnkyrinG is required to maintain axo-dendritic polarity *in vivo*. Proc Natl Acad Sci U S A 106:17564–17569. CrossRef Medline

Subramanian R, Kapoor TM (2012) Building complexity: insights into self-organized assembly of microtubule-based architectures. Dev cell 23: 874–885. CrossRef Medline

Tseng WC, Jenkins PM, Tanaka M, Mooney R, Bennett V (2015) Giant ankyrin-G stabilizes somatodendritic GABAergic synapses through opposing endocytosis of GABAA receptors. Proc Natl Acad Sci U S A 112: 1214–1219. CrossRef Medline

Yoshimura T, Rasband MN (2014) Axon initial segments: diverse and dynamic neuronal compartments. Curr Opin Neurobiol 27:96–102. CrossRef Medline

Zhang X, Bennett V (1998) Restriction of 480/270-kD ankyrin G to axon proximal segments requires multiple ankyrin G-specific domains. J Cell Biol 142:1571–1581. CrossRef Medline

Zhou D, Lambert S, Malen PL, Carpenter S, Boland LM, Bennett V (1998) AnkyrinG is required for clustering of voltage-gated Na channels at axon initial segments and for normal action potential firing. J Cell Biol 143: 1295–1304. CrossRef Medline